Journal of the Korean Physical Society, Vol. 73, No. 3, August 2018, pp. 368∼376

A Proof-of-Concept Study for the Real-Time Prediction of Respiratory Patterns: a Simple Bayesian Approach

Kwang-Ho Cheong, Sei-Kwon Kang,* Jai-Woong Yoon, Soah Park, Taejin Hwang, Me Yeon Lee, Tae Ryool Koo, Haeyoung Kim, Kyoung Ju Kim, Tae Jin Han and Hoonsik Bae
Department of Radiation Oncology, Hallym University College of Medicine, Anyang 14068, Korea

(Received 30 April 2018, in final form 26 June 2018)

Recent radiation therapy has overcome the effect of internal organ motion by limiting the range of movements, gating the beam irradiation or tracking the target movement. A successful strategy requires accurate real-time estimation of target location during radiation treatment. In this study, we propose a relatively simple technique to predict patient's respiratory pattern (RP) one step before the breathing using a Bayesian approach. Patients' respiratory signals (RSs) were analyzed using the in-house RPM signal analyzer, and parameters (period (τ), baseline (β) and amplitude (φ)) characterizing an RP were extracted. Based on each parameter, we obtained the probability density function (PDF) and transition probability matrix defined as 'likelihood'. We predicted the following RP based on the PDF and the likelihood, then compared the estimated RP with the actual one. The proposed method was applied to five lung cancer patients who were treated with radiation therapy in our facility. Prediction error was analyzed using root-mean-square error (RMSE;ε, in mm) and relative RMSE (ϵ, in %) for each breathing cycle in all RP. The ε range was [0.45,2.66], and ϵ range was [5,18.8]. The prediction accuracy was strongly dependent on the irregularity of RP. Although the prediction errors were more significant than expected, we could confirm the feasibility of the proposed algorithm. The proposed algorithm is more intuitive than other sophisticated methods and requires less computation time.

PACS numbers: 87.55.−x, 87.55.Gh, 87.55.K−, 87.19.Wx, 02.50.−r
Keywords: Radiation therapy, Lung cancer, Respiratory pattern, Bayesian inference, RPM system
DOI: 10.3938/jkps.73.368

I. INTRODUCTION

Traditionally, radiation therapy treats targets those are assumed to be static; however, internal organ motion, as well as targets especially during respiration, complicates the situation. Recent radiation therapy has overcome the effect of internal organ motion by limiting the range of movements [1,2], gating the beam irradiation [3, 4] or tracking the target movement [5–7]. A successful strategy requires accurate real-time estimation of target location during radiation treatment.

Surrogates of patients' surface were used widely to estimate the target motion indirectly because observation of target motion is not straightforward. Even though the correlation between the surrogate and the target motion is not substantial as expected [4,7], still it is most widely used clinically due to its simplicity and ease of use. A more direct approach entails the use of x-ray imaging with fiducial markers inside or around the target [8] for accurate but inconvenient and invasive analysis, resulting in additional radiation exposure. Either way, respiratory signals (RSs) are obtained before or during the treatment, and these signals exhibit a specific pattern in each patient.

Various methods were proposed to predict the respiratory pattern (RP) for decades. Most typically, the methods were based on statistical analysis, especially time series analysis. Auto-regression or moving average was the most widely used in early days of respiratory prediction [9,10]. However, simple statistical methods cannot guarantee appropriate clinical application without determining the relationship between each respiration period. More advanced techniques include signal processing applications such as Kalman filtering [11,12], ridge regression [13] or wavelet analysis [14]. Currently, machine learning techniques such as support vector machine [13, 15] and neural networks [16, 17] especially, deep learning aid in the effective resolution [18]. However, these methods require substantial computing time due to its complexity, even some of them is difficult to be applied for online real-time prediction of target motion since the computation time for predicting point is longer than the sampling rate of acquiring RSs [18]. Moreover, the formerly proposed algorithms are typically point-prediction

*E-mail: seikang@hallym.or.kr

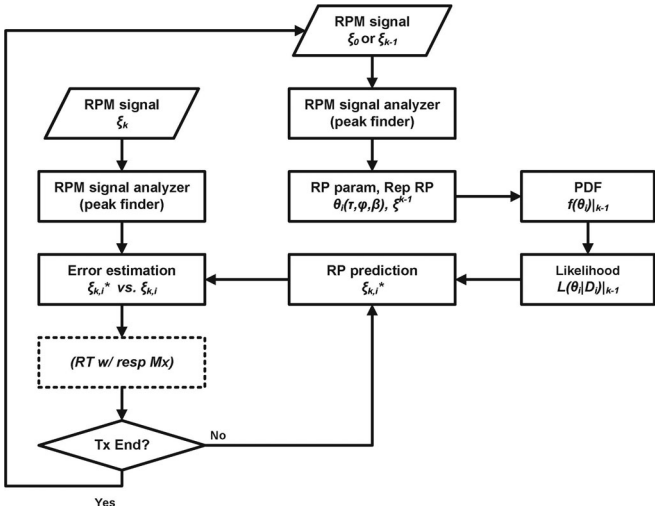

Fig. 1. Overall workflow of the study. Detailed symbols and formulae are described in Secs. II.2 to II.5. RP stands for a 'respiratory pattern', $k-1$ implies cumulated respiratory signals with $\{\xi_k\}_{k=0}^{k-1}$; RP parameters (shortened as 'param') and representative (shortened as 'Rep') RP were generated based on $\{\xi_k\}_{k=0}^{k-1}$. RP prediction module estimated a subsequent RP using a Bayesian inference based on the probability density function (PDF) and the likelihood function, which were pre-calculated. Actually, radiation therapy with respiration management (Mx) was not implemented in this study.

approach rather than forecasting a whole RP; it is hard to seize the pattern of the upcoming RS at a glance.

In this study, we propose a relatively fast and simple technique to predict patient's RP using a Bayesian approach also known as 'conditional probability' that is expressed as $P(Y|X)$ or '*probability of Y if given X condition*'. Bayesian inference is based on the Bayesian theorem and can be used for addressing real-world problems efficiently [19]. The main idea of the study is to select the most probable parameters characterizing the RP in one step before each breathing cycle based on the Bayesian inference considering RPs past and just before with gathering RS in real-time.

II. MATERIALS AND METHODS

1. Idea and workflow

Figure 1 outlines the overall workflow of the study. We analyzed patients' RSs using the in-house RPM signal analyzer and extracted the parameters characterizing an RP. Based on each parameter, we obtained the probability density function (PDF) and transition probability matrix defined as likelihood function or merely 'likelihood'. We then predicted the following RP based on previous RP. Finally, we compared the estimated RP with the actual one. The PDF and likelihood were calculated before prediction of the RP. Thus, the computation time of Bayesian inference is required merely for 'prediction' of the procedure. However, radiation therapy with actual respiratory management was not implemented in this study.

The study idea is based on four assumptions: (1) Patients' RP is not much variant for intra- and inter-fractional series, but just scaled from the representative model of unit respiration. Our previous study supports this assumption [20]. (2) Even though the characteristic parameters vary with time, they are distributed in a limited range except for extreme outliers. Typically, they are modeled by a Gaussian distribution. (3) Regarding RSs, the preceding breathing pattern influences the successive pattern, and is known as 'transition'. Furthermore, the distribution of each breathing pattern is not sporadic, instead, it follows hidden rules. Therefore, knowledge of the distribution of the parameters representing an RP and distribution of the probability of transition from one endpoint to the next parameter, facilitates the prediction of subsequent RPs. (4) Even if there were a significant discrepancy between the amplitude of the models, the estimated error in the position would be less than clinically acceptable. These four assumptions might be understood intuitively.

2. Analysis of respiratory signals

In this section, we briefly explain how to analyze RSs and to extract parameters those characterize an RP. RS analysis is required for procedures to generate base data, statistical analysis, and predicting and validation. In this study, we used the Real-time Position Management^{TM} (RPM) system (Varian Medical Systems, USA) to determine the RSs. The RPM system records the RS with a frequency of 30 Hz. We extracted the RSs those obtained during CT simulation and treatment with gating technique. We then used MatLab 2017b (MathWorks Inc., USA) for signal processing and statistical analysis including prediction and validation.

Before analysis of the RSs, all the signals were shifted to the centerline at 0, because of inter-fractional variation in the ranges of marker positions. We used 'peak-finding method' that was introduced in our previous study to analyze the RSs and to determine the peaks(x mark) and valleys(o mark) as shown in Fig. 2 and defined as "peak-to-peak" (one end-of-exhalation (EE) to the next EE) as one respiratory period [20].

RP is characterized using multiple parameters such as time interval between inhalation and exhalation (period or frequency), the range of a marker or target position (amplitude), the phase of the breathing cycle, and so forth. In this study, we defined a few notations to clarify the logic in this manuscript.

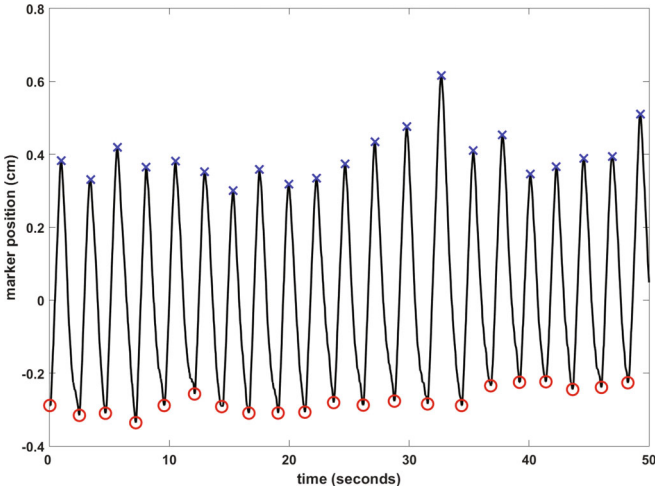

Fig. 2. (Color online) RPM system with the 50-s respiratory signal of $\xi_{m=1,k=0}$. The raw data were flipped upside down and appeared to the centerline 0 for convinence. The amplitude was not renormalized because the RPM system normalized the signal to the actual motion range against the known distance between two dots on the marker. The peaks at the end of exhalation (o mark) and inhalation (x mark) estimated using the 'peak finder' were displayed as well.

- respiratory signal (RS, ξ_k): raw or processed respiratory data obtained at a k'th fraction of radiotherapy
- unit respiratory signal ($\xi_{k,i}$): decomposed ξ_k for one period; i denotes i'th unit RS of ξ_k
- respiratory pattern (RP): variation, characteristic or regularity of ξ_k; generally, RP is estimated for overall ξ_k, however, we applied that concept to $\xi_{k,i}$ to distinguish the term 'respiratory pattern' from 'respiratory signal'.
- period(τ): from the EE to the next EE or duration time of $\xi_{k,i}$, determined as time (s)
- baseline(β): the lowest position of the marker in $\xi_{k,i}$; generally, at the EE. determined as position (cm)
- amplitude(φ): defined with positions of the marker, from the baseline to the highest position in $\xi_{k,i}$, determined as a range (cm)

To facilitate visual comprehension, we employed a virtual box concept as shown in Fig. 3 as ξ_k is a consecutive stacking of the virtual boxes. We define a new variable θ that is a parametric function of τ, φ and β; θ is rewritten as $\theta(\tau, \varphi, \beta)$. Therefore, $\xi_k = \{\xi_{k,i}\} = \{\xi_k(\tau_i, \varphi_i, \beta_i)\} = \{\xi_k(\theta_i)\}$. Here, we assumed that τ, φ, and β are independent of each other. Thus, the variables were treated separately. In this paper, θ was also used as a representative expression of individual τ, φ, and β in some cases.

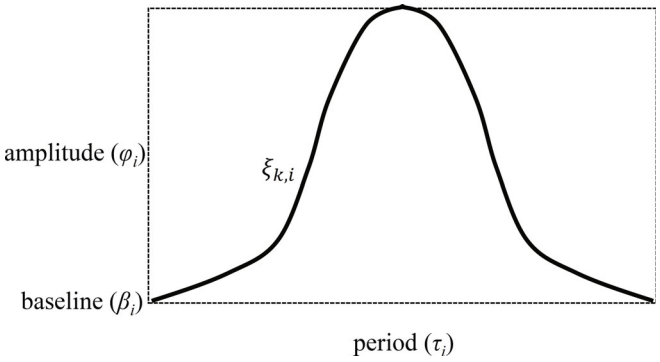

Fig. 3. Virtual box concept employed for visual comprehension. A unit respiratory pattern of a k'th breathing cycle is denoted as $\xi_{k,i}$, while the period, amplitude and the baseline are expressed as τ_i, φ_i and β_i repectively. ξ_k is a series of $\xi_{k,i}$, thus, $\xi_k = \{\xi_{k,i}\} = \{\xi_k(\tau_i, \varphi_i, \beta_i)\}$.

We collected a total of 55 RSs from five lung cancer patients who were treated with radiation therapy in our facility. They were 11 signals per patient; one during four-dimensional (4D) computed tomography (CT) scanning for radiation therapy planning (ξ_0) and 10 for randomly selected radiation therapy fractions in order, thus $PT_m = \{\xi_{m,k}\}$, where m is a patient index such that $m \in \{1, 2, 3, 4, 5\}$, while $k \in \{0, 1, 2, \cdots, K, \cdots, 9, 10\}$. However, m was not indicated in this manuscript except when necessary.

3. Generating representative unit respiratory pattern

This section describes how to generate a basic or representative unit RP using previously obtained RSs. The algorithm proposed in this study simply states that 'scaling a representative unit respiratory pattern', which is defined as ξ^k, by adjusting τ, φ and β as much as predicted. For example, ξ^0 is modeled by averaging $\{\xi_i\}_{k=0}$ whose phase is normalized to $[0, 2\pi]$ with 100 sampling points since $\tau_{k,i}$ is a variant for all $\xi_{k,i}$. Furthermore, the irregularity among $\{\xi_{k,i}\}$ plays a nuisance role that spoils the representative nature of respiration. Our previous report was intended to estimate the irregularity of respiration [20]. An example of ξ^0 is presented in Fig. 4.

In the first application of the prediction algorithm to the first treatment fraction, we used ξ^0. However, ξ^0 was updated to ξ^K as fractions progressed by averaging $\{\xi_i\}_{k=0}^K$.

4. Bayesian approach to prediction of the respiratory pattern

We describe the main part of the plan (Bayesian prediction module) in this section. A key point of the pro-

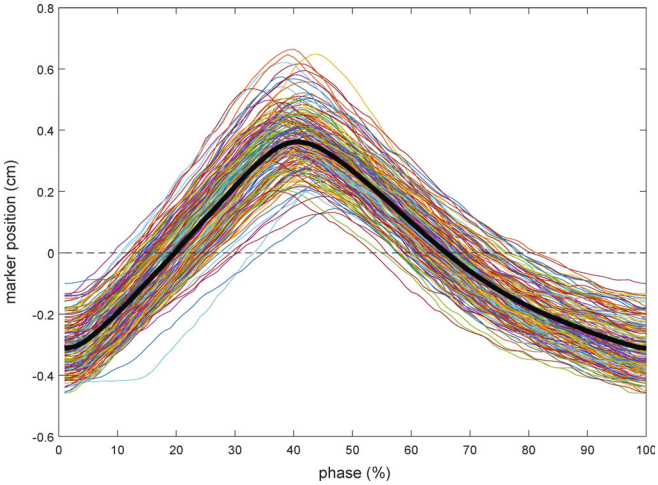

Fig. 4. (Color online) Example of a representative respiratory pattern (ξ^0, thick black line) generated by averaging $\{\xi_(0,i)\}_{m=1}$ (thin, colored lines) for the first application of the prediction algorithm to the first treatment fraction ($k=1$). ξ^0 was updated to ξ^K as fractions proceed by averaging $\{\xi_k\}_{k=0}^{K}$.

posed algorithm is to estimate the most probable parameter by considering $\{\xi_{k,i}\}_{i=1}^{i-1}$. If we estimate θ_i^*, then $\xi_i^* = \xi(\theta_i^*)$ at a k'th fraction. In other words, if previous $\{\tau_{i-n}\}, \{\varphi_{i-n}\}$ and $\{\beta_{i-n}\}$ (n is an arbitary number) are continuously provided, we can estimate the τ_i^*, φ_i^* and β_i^* respectively.

In this study, we employed a Bayesian approach to estimate θ_i^*. Based on the Bayesian theorem, $P(\theta_i|D_i)$ is espressed as Eq. (1):

$$\begin{aligned} P(\theta_i|D_i) =& \frac{P(D_i|\theta_i)P(\theta_i)}{P(D_i)} \\ =& \frac{P(D_i|\tau_i,\varphi_i,\beta_i)P(\tau_i,\varphi_i,\beta_i)}{P(D_i)}, \end{aligned} \tag{1}$$

where $P(D_i|\theta_i)$ is known as the 'likelihood function' and $P(\theta_i)$ is a prior-probability already known and $D_i = \{\xi_{k,i}\}_{i=1,k=1}^{i-1,k-1}$.

Bayesian inference is composed of three procedures: prior-probability, likelihood, and posterior-probability. We determined each term as follows:

- prior-probability: PDF of θ_i; $f(\theta_i)$
- likelihood: transition probability; $f(D_i|\theta_i) \equiv L(\theta_i : D_i)$
- posterior-probability: θ_i^* that satisfies Eq. (2),

$$\theta_i^* = \arg\max_{\theta_i}\{P(\theta_i|D_i)\} = \arg\max_{\theta_i} f(D_i|\theta_i)f(\theta_i), \tag{2}$$

θ_i^* is the most probable choice among the probability density or distribution to a specific condition needs to be determined. The Eq. (2) can be rewritten as Eq. (3):

$$\begin{aligned} \theta_i^* &= \arg\max_{\theta_i}\{P(\theta_i|D_i)\} \\ &\propto \int P(\theta_i|\theta_{i-1},\cdots,\theta_1)\times P(\theta_1,\cdots,\theta_{i-1}|\theta_i)d\theta_i. \end{aligned} \tag{3}$$

In here, $P(\theta_i|\theta_{i-1},\cdots,\theta_1) \cong f(\theta_i)$ and $P(\theta_1,\cdots,\theta_{i-1}|\theta_i) \cong L(\theta_i : D_i)$. $f(\theta_i)$ was updated after every fraction of radiation treatment; newly obtained actual RS was added to previously processed data. $L(\theta_i : D_i)$ was defined as a 'transition probability matrix'; the term 'transition probability' stands for $P(\theta_i \to \theta_{i+1})$. The same concept was applied to τ, φ and β respectively. To generate $f(\theta_i)$, we used a histogram of θ_i itself that is defined as $\mathbb{H}(\theta_i)$ to preserve the raw distribution attributes, even though it is reasonable to assume that distributions of θ_i follow Gaussian distribution as $\tau \sim N(\mu_\tau,\sigma_\tau), \varphi \sim N(\mu_\varphi,\sigma_\varphi), \beta \sim N(\mu_\beta,\sigma_\beta)$. For the latter fraction, the $f(\theta_i)$ was generated using all ξ upto $k-1$.

To generate $\mathbb{H}(\theta_i)$, we discretized each distribution into a specific number (Θ) of bins. Naturally, it is accomplished by generating a histogram from 0 to the maximum number by dividing with Θ; however, if the range of $[0,\max]$ is too broad due to outliers, it is reasonable to limit scope to 95^{th} percentile data (2σ in the Gaussian distribution) to encompass 95% RPs in the analysis. The outside values of the range were coded as 0 ($<(\mu_\theta - 2\sigma_\theta)$) and $\Theta+1$ ($>(\mu_\theta+2\sigma_\theta)$) respectively. This method was applied to τ, φ and β, respectively. Then, Θ was determined by $\Theta = 4\sigma/\delta$ where δ is a user-defined bin size that implies a resolution of time or length. The smaller δ produced a large number of bins, and required heavy computation time. Furthermore, if ξ_k is not long enough or statistically meaningful, increasing δ might elicit a significant error. Therefore, we need to adjust δ to a reasonable level. The final form of $f(\theta_i)$ has a $1\times\Theta$ matrix.

$L(\theta_i : D_i)$ was generated by counting a frequency of $\theta_a \to \theta_b$ as Eq. (4),

$$L_{a,b} = \text{frequency}(\theta_a \to \theta_b), \tag{4}$$

where $a,b \in \{1,2,\cdots,\Theta\}$ for $i-1$ and i respectively, and yields $Theta \times \Theta$ matrix. The $L_{a,b}$ was normalized to $\sum_{a=1}^{\Theta}\sum_{b=1}^{\Theta} L_{a,b} = 1$. Because the RPs before $\xi_{k,i-1}$ also affect $\xi_{k,i}$, we need to consider the formers. Then $L(\theta_i : D_i)$ considering l'th backward becomes Eq. (5),

$$L(\theta_i : D_i) = \prod_{l=1}^{i-1} L(\theta_i : D_i)_l. \tag{5}$$

However, it is not practicable to calculate $L(\theta_i : D_i)$ for all l until i, even though it was calculated before the prediction. We calculated for a limited number(η) of previous $\xi_{k,i}$ since the older data were less informative than

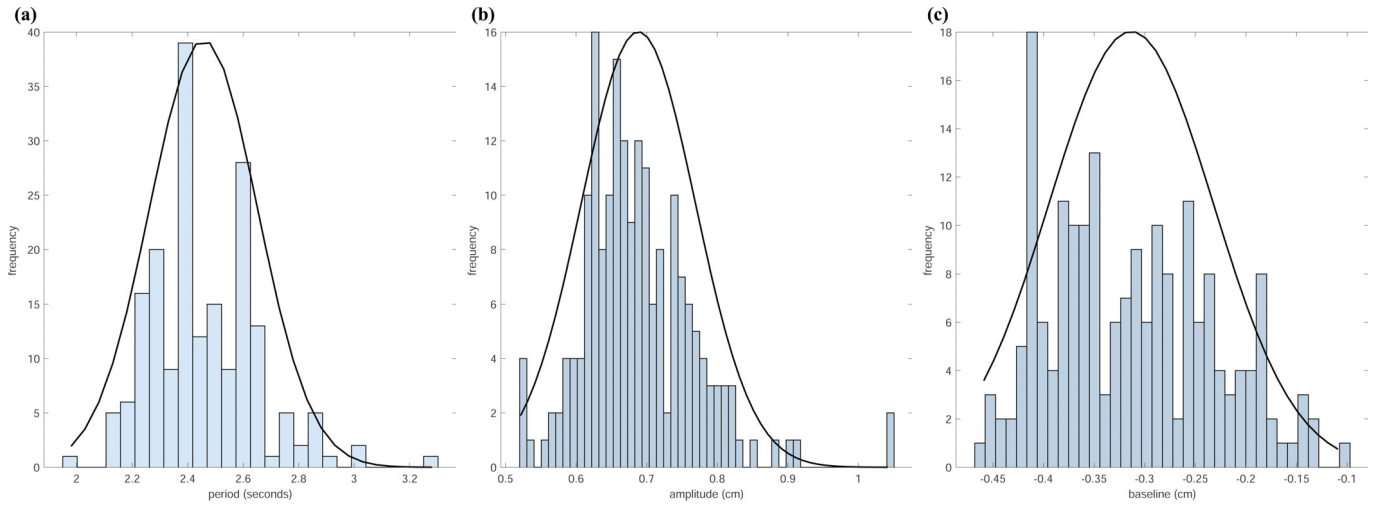

Fig. 5. (Color online) A graphical example of $f(\theta_i)$ for τ, φ and β of $\xi_{i_{k=1,m=1}}$. $k = 0$ implies that it was generated from the data obtained during the CT simulation. Here, we adjusted the values of $\delta_\tau = 0.05$ sec, $\delta_\varphi = 0.01$ cm and $\delta_\beta = 0.02$ cm respectively to ensure Θ of each parameter around 30; for example, numbers of bins used to generate $\mathbb{H}(\theta_i)$ with regard to τ, φ and β were $\Theta_\tau = 31$, $\Theta_\varphi = 32$ and $\Theta_\beta = 35$ in this case.

the new data. Therefore Eq. (5) is rewitten as Eq. (6),

$$L(\theta_i : D_{i-\eta})_\eta = \prod_{l=i-\eta}^{i-1} L(\theta_i : D_i)_l. \tag{6}$$

The Eq. (3) is expressed as Eq. (7),

$$\begin{aligned}\theta_i^* &= \arg\max_{\theta_i}\{P(\theta_i|D_{i-\eta})\} \\ &\propto \iint P(\theta_i|\theta_{i-1},\cdots,\theta_1) \\ &\qquad \times P(\theta_{i-\eta},\theta_{i-\eta+1},\cdots,\theta_{i-1}|\theta_i)d\eta d\theta_i. \end{aligned} \tag{7}$$

Finally, we obtained a distribution of $\hat{\theta}_i$ for η iterations, θ_i^* is the most probable value consdiering $\{\theta_{i-1},\cdots,\theta_{i-\eta}\}$. This process is repeated to predict τ_i^*, φ_i^* and β_i^*.

5. Comparison between predicted and actual respiratory data

Finally, we explain how to evaluate the accuracy of the predicted RPs by comparing with the actual one in this section. The system records actual and predicted data altogether for verification. For practical purpose, ξ_i^* was connected continuously based on the actual $\xi_{k,i}$ since the $\xi_{k,i}^*$ is only valid for i'th breathing cycle. As shown in Fig. 3, the virtual boxes were arranged on the baseline (β_i^*), and scaled by applying τ_i^* and φ_i^*. Every starting point of the ξ_i^* was corrected to the end point of the actual ξ_{i-1} to decrease the cumulative error. In other words, $\xi_{k,i}$ and $\xi_{k,i}^*$ have a same starting point.

To achieve the study goal, each $\xi_{k,i}^*$ needs to be compared with the $\xi_{k,i}$ for a new k in real time. However, this study was intended to prove the idea and is a retrospective study, we supposed that ξ_{k+1} was a new and unknown data. To estimate the error between actual and predicted signal, we employed root-mean-square error (RMSE) for error analysis. First, RMSE for a $\xi_{k,i}$ is defined by Eq. (8) as follows:

$$\varepsilon_i = \sqrt{\frac{1}{N_i}\sum_{n=1}^{N_i}(\xi_{k,i,n}^* - \xi_{k,i,n})^2}, \tag{8}$$

where n is a sampling point of each $\xi_{k,i}(t)$, whose total number of sampling points is denoted by N_i. In other words, ε_i is a positional discrepancy at time t. Therefore, the unit of the ε_i is length, *i.e.* millimeters. Next, we applied mean and standard deviation of $\{\varepsilon_i\}_k$ for the overall estimation of RMSE for ξ_k. The former was defined as a global error (ε_k). We also employed the concept of relative RMSE (ϵ_k) that is defined as Eq. (9):

$$\epsilon_k = \frac{\varepsilon_k}{\bar{\varphi}_k}, \tag{9}$$

where $\bar{\varphi}_k$ is a averaged amplitude of ξ_k. ϵ_k is a percentage error to the amplitude, and is intended to consider the different $\bar{\varphi}_k$ of each ξ_k. We analyzed ε_k and ϵ_k for all patients and fractions. In some cases, the RP is non-standard due to a cough or deep inspiration, that respiration is ignored and not used in the analysis or update of the procedures for the calculation of $f(\theta_i)$ and $L(\theta_i : D_i)$, but used for the evaluation of the prediction accuracy.

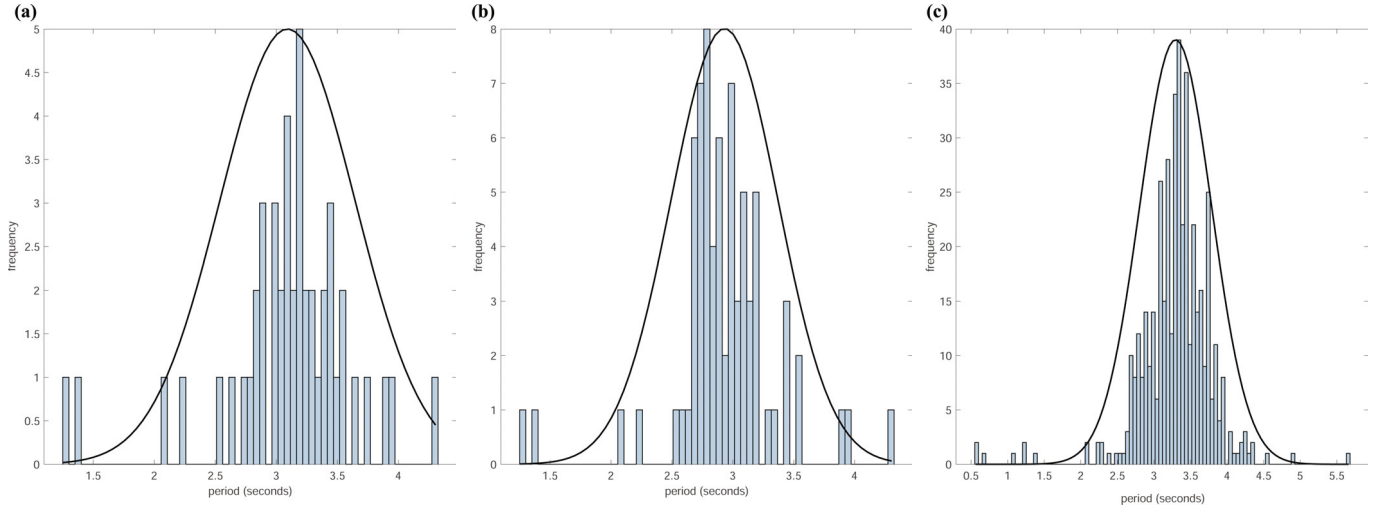

Fig. 6. (Color online) $f(\tau_i)$ of (a) ξ_0 only, (b) ξ_{0+1} and (c) $\xi_{0\sim9}$ for $m = 2$. Larger volume of data make the Gaussian distrubution narrower compared with less data. However, tails of the distribution were much longer than small k.

III. RESULTS

1. Calculation of prior-probability and likelihood

Figure 5 is a graphical example illustrating $f(\theta_i)$ for τ, φ and β of $\xi_{ik=1,m=1}$. Here, we adjusted the value of $\delta_\tau = 0.05$ sec, $\delta_\varphi = 0.01$ cm and $\delta_\beta = 0.02$ cm respectively, to obtain Θ of each parameter around 30. For example, the numbers of bins used to generate $\mathbb{H}(\theta_i)$ with regard to τ, φ and β were $\Theta_\tau = 31$, $\Theta_\varphi = 32$ and $\Theta_\beta = 35$ in this case. Because τ is more critical than φ and β when predicting RP generally, it needs appropriate adjustment for δ. Figure 6 presents the value of $f(\tau_i)$ with (a) ξ_0 alone, (b) ξ_{0+1} and (c) $\xi_{0\sim9}$ for $m = 2$. Apparently, a higher number of data leads to narrower Gaussian distrubution compared with fewer data. However, the tails of distribution were much longer than small k. If the observations are centered on the mean of the Gaussian distribution, it is the most probable period occurring most frequently. However, mere PDF does not guarantee the robustness of the probability. Therefore, we employed the likelihood that was generated using a transition probability. If $L(\theta_i : D_i)$ is maximized, it yields the most probable parameter.

Based on Eq. (6), $L(\theta_i : D_{i-\eta})_\eta$ for former $\xi_{k,i}$ is estimated by multiplying itself during prediction procedure. However, after specific η, $L(\theta_i : D_{i-\eta})_\eta$ has relatively small probability and contributes to the prediction of ξ_i^* less than the newer one. Nevertheless, coefficients in the matrix converged into specific probability after approximately 10 iterations; it stands for that $\hat{\theta}_i$ using $\eta > 10$ does not contribute to increase the prediction accuracy, rather increase just calculation time. For $\eta < 10$, even for less η, distribution of $\hat{\theta}_i$ was scattered than that of more η, thus it was relatively hard to estimate θ_i^*. Therefore, we concluded that $\eta = 10$ was optimal for the study.

Table 1. Prediction error analysis (global error (ε)) using root-mean-square error (mm)) for all $\{\xi_{m,k}\}$ (m denotes a patient index while k implies a treatment fraction index).

m \ k	1	2	3	4	5
1	0.48	0.86	1.38	0.76	1.70
2	0.87	0.60	1.21	0.89	2.19
3	1.13	0.67	1.02	0.58	2.66
4	0.46	0.50	1.16	0.92	1.71
5	0.60	0.73	0.92	0.81	1.49
6	0.80	1.10	1.18	0.64	1.03
7	0.51	1.30	1.82	0.90	1.29
8	0.77	0.70	1.62	0.83	1.23
9	0.68	0.86	0.95	0.79	1.38
10	0.45	1.03	1.28	0.74	1.23

2. Discrepancy analysis between actual and predicted respiratory pattern

Figure 7(a) shows a comparison between prior potions of the predicted ($\xi^*_{m=1,k=1}$) and the actual ($\xi_{m=1,k=1}$) RPs. In fact, as the first part of ξ_k is used for short training for prediction, those periods were not used for evaluation. Figure 7(b) highlights the differences of the predicted and actual marker position. Time shift and the difference in the peak induced significant error in the prediction; the error was as much as 2 mm. The effect of β was relatively small than the others although the distribution of β was most wide-ranging shown in Fig. 5(c).

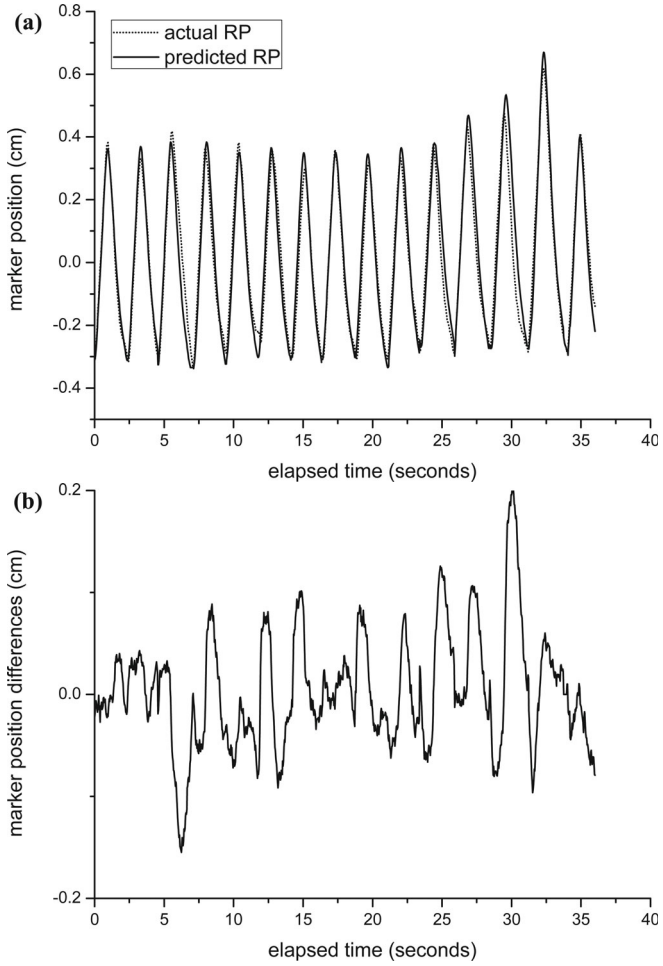

Fig. 7. (a) Predicted (ξ_k^*; solid line) and actual (ξ_k; dotted line) respiratory pattern of $\xi_{m=1,k=1}$ and (b) differences of predicted and actual marker positions.

Prediction errors expressed in ε_k and ϵ_k for all $\{\xi_{m,k}\}$ are summarized in Tables 1 and 2 respectively. The case in Fig. 7, $\varepsilon_{m=1,k=1}$ was 0.48 mm and 8.0 % to the $\varphi_{m=1,k=1} = 6$ mm. In all cases, the ε_k range was [0.45,2.66] and the ϵ_k range was [5,18.8]. Maximal ε_k implies that the proposed algorithm has an error limitation of mean 2.66 mm in estimating target position in real time. This error was relatively larger than expected, however, we could confirm the feasibility of the proposed algorithm.

Although $f(\theta_i)$ and $L(\theta_i : D_i)$ in case of cumulative ξ_k with increased k have more obvious features than less k, ε_k using increased cumulative k was not decreased significantly since the prediction accuracy was strongly dependent on the irregularity of RP. However, it is apparent that the more (cumulated) observed data supports the accurate prediction for the same RS.

Table 2. Relative prediction error analysis (ϵ_k) in percentage (%) to the averaged amplitude (φ_k) for all $\{\xi_{m,k}\}$ (m denotes a patient index while k implies a treatment fraction index).

m \ k	1	2	3	4	5
1	8.0	8.6	9.2	7.6	13.1
2	12.4	6.0	9.3	6.8	12.1
3	18.8	8.3	6.8	5.8	14.8
4	7.6	5.0	9.7	8.4	9.5
5	8.6	8.2	6.2	10.1	9.9
6	11.4	10.0	8.5	8.0	7.4
7	8.5	14.4	13.0	8.2	8.6
8	11.0	8.7	16.2	8.3	8.2
9	8.6	12.3	6.8	7.1	8.1
10	6.4	12.9	12.8	8.2	8.2

IV. DISCUSSION

Our goal in this study was to establish a simplified prediction of RP in real time using Bayesian approach. Toward this end, we made several assumptions as described in Sec. II.1. Some of the assumptions need to be qualified, but practically, these assumptions are valid as long as the patient has a regular RP in a tolerable range.

To the best of our knowledge, the Bayesian approach was not utilized extensively to predict the RP by other studies. However, Bayesian methods have been widely used in various fields as well as in medical application [21–23]. Application of the Bayesian approach to the time series, especially to predict the following pattern is still a challenge [19, 23]. In this study, we showed the possibility of predicting the subsequent RP based on a prior cycle; however, the expected RP did not match adequately. The error was severe when the patients' RP was irregular.

Our method has specific limitations. First, although the amplitude of a unit RS of a surrogate is assumed to reflect the entire range of actual target motion, they do not match perfectly due to the interplay and lag in signal acquisition, resulting in serious errors in the estimation of the target motion [6,7,24]. However, this study was intended to prove the concept of prediction of RP using simple Bayesian inference. The proposed algorithm can be applied to acquire RSs from any device. Second, we used one-dimensional (1D) RS in the superior-inferior (SI) direction excluding the possibility of prediction in the other directions, and was attributed to the limitation of the RPM system used. However, the SI directional movement is most significant with potential clinical applications [4,7,13]. Third, although the overall RP might vary from session to session (inter-fractional difference), the method is valid as long as the pattern of unit respiration is sustained. Fourth, we assumed that τ, φ, and

β were independent and treated them as independent variables. However, when we investigated the correlation between τ and φ for the RSs used in the study, the Pearson's correlation coefficient between them was estimated about $0.2 \sim 0.7$; these numbers were above our expectation while the correlation does not seem to affect to the prediction of the other parameters. Even though we didn't confirm effects of the correlation, we will study about this issue in future. Finally, we admit that the patient cohort was tiny; however, this study is a proof-of-concept purpose and requires less significance in a statistical meaning. Moreover, even the number of the patients was 5, number of RSs used in this study was 50 in fact. Thus, we regarded it was reasonable to verify the proposed methods with these amount of data in this stage.

We believe that our method is more intuitive than other methodologies. The two primary processes in this study were used to generate ξ^0 and pre-calculate $f(\theta_i)$ and $L(\theta_i : D_{i-\eta})_\eta$ before the prediction procedure. Even though the calculation of $f(\theta_i)$ and $L(\theta_i : D_{i-\eta})_\eta$ is rapid, real-time updates require additional time more than the lag allowed between data acquisition and prediction, suggesting the need for reasonable computation in advance. We did not use the complex Bayesian methods such as Markov chain Monte Carlo (MCMC) or Hidden Markov model (HMM) [25]. Rather, we employed a limited sampling of the Bayesian theorem considering a few previous breathing cycles for a fast prediction. The prediction by the module was comparable to other methods.

Predicting RP is still a challenge in the management of patients' target motion. However, there is no "gold standard" available. The difficulty is attributed to the randomness and irregularity of breathing. Irregular RP complicates the forecast of the actual target position. Bukhari *et al.* predicted respiratory motion using extended Kalman filters (EKF) and Gaussian process regression network (GPRN) [12]. They used a GPRN (a nonparametric Bayesian algorithm for modeling correlations between the output variables) to correct the prediction error of the EKF in 3-dimensional space. Putra *et al.* suggested a multiple model approach to respiratory motion prediction for real-time IGRT [26]. They employed the interacting multiple model (IMM) and proposed a confidence interval (CI) criterion to evaluate the performance of tumor motion prediction algorithms. They also showed that 95% CI criterion is an effective margining strategy to accommodate prediction errors. A probability-based approach was implemented by Kalet *et al.* and Ruan *et al.* Kalet *et al.* reported a state-based probabilistic model for tumor respiratory motion prediction [25]. In their study, tumor motion was broken down into linear breathing states and sequences of states. They adopted an HMM to predict the future sequences by analyzing breathing state sequences and the observables. They presented an increased average duty cycle using the HMM comparing to other methods, while predicted state sequences were well correlated with sequences known to fit the data. Ruan *et al.* used a kernel density estimation-based real-time prediction [27]. Like our method, they tried to obtain a distribution of the target position based on the previous sample values by estimating the joint PDF of the covariate (observed) and response (predicted) variables using an efficient kernel density estimation method. However, their approach was limited to less than 1-second forecasting, and the predicting accuracy was dependent on the sampling rate. We focused on the calculation time for real-time prediction, a compromise between calculation time and accuracy regardless of the sampling rate. The simple algorithm facilitates prediction of real-time RP owing to less computational load. We do not deny the feasibility of real-time prediction using all the formerly reported methods. However, we could not find enough evidence of the real-time possibility of them through the literature survey. Although proof of the real-time feasibility does not seem to be easy because of the complexity of situations in the clinic, computation time can be a barometer. The calculation times for an upcoming point using the previously reported prediction algorithms was $1.5 \sim 250$ ms [18]; some algorithm is slower than the sampling rate. Mere calculation time for a prediction of an RP using our method was less than 1 seconds, with MatLab code and Core i7 Laptop computer; optimization of the code and better computing power will enhance the efficiency of the algorithm. We guess that it is enough time to predict and prepare to monitor the error for a respiratory cycle in real-time.

V. CONCLUSION

We showed a possibility of predicting patients' RP one step before the breathing by utilizing a simple Bayesian approach. The proposed algorithm is more intuitive than other sophisticated methods and requires less computation time. However, since this study is still work in progress, there is scope for improvement to develop more robust and feasible clinical applications.

ACKNOWLEDGMENTS

This work was supported by Radiation Technology R&D program through the National Research Foundation of Korea funded by the Ministry of Science and ICT (No.2016M2A2A7952291).

REFERENCES

[1] B. Gagel *et al.*, Int. J. Radiat. Oncol. Biol. Phys. **67**, 742 (2007).

[2] A. Betgen, T. Alderliesten, J. J. Sonke, C. Van Vliet-Vroegindeweij, H. Bartelink and P. Remeijer, Radiother. Oncol. **106**, 225 (2013).
[3] G. D. Hugo, N. Agazaryan and T. D. Solberg, Med. Phys. **29**, 2517 (2002).
[4] H. Wu, Q. Zhao, R. I. Berbeco, S. Nishioka, H. Shirato and S. B. Jiang, Phys. Med. Biol. **53**, 7137 (2008).
[5] T. Krilavicius, I. Liobaite, H. Simonavicius and L. Jaruevicius, in *Proc.- IEEE Symp. Comput. Med. Syst.* (2016), p. 7.
[6] K. Poels *et al.*, Radiother. Oncol. **112**, 352 (2014).
[7] D. Ionascu, S. B. Jiang, S. Nishioka, H. Shirato and R. I. Berbeco, Med. Phys. **34**, 3893 (2007).
[8] S. Shimizu *et al.*, Int. J. Radiat. Oncol. Biol. Phys. **81**, e393, (2011).
[9] R. Dürichen, T. Wissel and A. Schweikard, Int. J. Comput. Assist. Radiol. Surg. **8**, 1037 (2013).
[10] D. Cervone, N. S. Pillai, D. Pati, R. Berbeco and J. H. Lewis, Ann. Appl. Stat. **8**, 1341 (2014).
[11] W. Bukhari and S. M. Hong, Phys. Med. Biol. **60**, 233 (2015).
[12] W. Bukhari and S-M. Hong, Phys. Med. Biol. **61**, 1947 (2016).
[13] A. Krauss, S. Nill and U. Oelfke, Phys. Med. Biol. **56**, 5303 (2011).
[14] R. Durichen, T. Wissel and A. Schweikard, Int. J. Comput. Assist. Radiol. Surg. **10**, 363 (2015).
[15] F. Ernst and A. Schweikard, Int. J. Comput. Assist. Radiol. Surg. **4**, 439 (2009).
[16] M. J. Murphy and S. Dieterich, Phys. Med. Biol. **51**, 5903 (2006).
[17] S-M. Hong and W. Bukhari, Phys. Med. Biol. **59**, 3555 (2014).
[18] S. Park, S. J. Lee, E. Weiss and Y. Motai, IEEE J. Transl. Eng. Heal. Med. **4**, 1 (2016).
[19] M. Van der Heijden, M. Velikova and P. J. F. Lucas, J. Biomed. Infrom. **48**, 94 (2014).
[20] K-H. Cheong *et al.*, J. Korean Phys. Soc. **66**, 301 (2015).
[21] R. Li, B. P. Fahimian and L. Xing, Med. Phys. **38**, 4205 (2011).
[22] D. Peressutti *et al.*, Med. Image Anal. **17**, 488 (2013).
[23] R. Dürichen, M. A. F. Pimentel, L. Clifton, A. Schweikard and D. A. Clifton, IEEE Trans. Biomed. Eng. **62**, 314 (2015).
[24] L. Court *et al.*, Med. Phys. **37**, 4 (2010).
[25] A. Kalet, G. Sandison, H. Wu and R. Schmitz, Phys. Med. Biol. **55**, 7615 (2010).
[26] K. Putra, D. Haas, O. C. L. Mills and J. A. Burnham, Phys. Med. Biol. **53**, 1651 (2008).
[27] D. Ruan, Phys. Med. Biol. **55**, 1311 (2010).